



Global malaria infection risk from climate change

Chao Li, Shunsuke Managi *

Urban Institute, Kyushu University, 744 Motooka, Nishi-ku, Fukuoka, 819-0395, Japan



ARTICLE INFO

Keywords:

Malaria
Climate change
Temperature
SSPs

ABSTRACT

As a long-standing public health issue, malaria still severely affects many parts of the world, especially Africa. With greenhouse gas emissions, temperatures continue to rise. Based on diverse shared socioeconomic pathways (SSPs), future temperatures can be estimated. However, the impacts of climate change on malaria infection rates in all epidemic regions are unknown. Here, we estimate the differences in global malaria infection rates predicted under different SSPs during several periods as well as malaria infection case changes (MICCs) resulting from those differences. Our results indicate that the global MICCs resulting from the conversion from SSP1-2.6 to SSP2-4.5, to SSP3-7.0, and to SSP5-8.5 are 6.506 (with a 95% uncertainty interval [UI] of 6.150–6.861) million, 3.655 (3.416–3.894) million, and 2.823 (2.635–3.012) million, respectively, from 2021 to 2040; these values represent increases of 2.699%, 1.517%, and 1.171%, respectively, compared to the 241 million infection cases reported in 2020. Temperatures increases will adversely affect malaria the most in Africa during the 2021–2040 period. From 2081 to 2100, the MICCs obtained for the three scenario shifts listed above are –79.109 (–83.626 to –74.591) million, –238.337 (–251.920 to –0.141) million, and –162.692 (–174.628 to –150.757) million, corresponding to increases of –32.825%, –98.895%, and –67.507%, respectively. Climate change will increase the danger and risks associated with malaria in the most vulnerable regions in the near term, thus aggravating the difficulty of eliminating malaria. Reducing GHG emissions is a potential pathway to protecting people from malaria.

Credit author statement

C.L. conducted the analyses and wrote the manuscript. S.M. conceived of the study and edited the manuscript. All authors reviewed the manuscript.

Ethics approval

Not applicable.

Role of the funding source

The funders had no role in the study design, data collection, data analysis, data interpretation, or writing of the report. The corresponding author had full access to all the data in the study and had final responsibility for the decision to submit for publication. All authors had access to the estimates presented in the paper.

1. Introduction

In many parts of this world, especially Sub-Saharan Africa, malaria transmission was high during the 2000–2019 period (Bhatt et al., 2015; WHO, 2021). The World Health Organization (WHO) estimated over 241 million infection cases in 85 countries and 627,000 malaria deaths in 2020, despite the implementation of various successful malaria-control interventions over the past 20 years (Bhatt et al., 2015; WHO, 2021). To achieve the established Sustainable Development Goals, the WHO set a series of ambitious aims, including reducing the global malaria incidence rate by at least 90% compared to the 2015 values and eliminating malaria in at least 35 countries in which malaria was transmitted in 2015 (WHO, 2021). In 2019, the *Plasmodium falciparum* parasite rate in 2- to 10-year-old children (PfPR₂₋₁₀) was still over 60% in many Sub-Saharan African regions, as shown by estimated data from ongoing mapping projects (Bhatt et al., 2015; Weiss et al., 2019). In this way, even without the interference of other factors, it will be difficult for the WHO to achieve its goals.

Climate change has been considered a factor altering the global

* Corresponding author. Kyushu University, 744 Motooka, Nishi-ku, Fukuoka, 819-0395, Japan.

E-mail address: managi@doc.kyushu-u.ac.jp (S. Managi).

pattern of malaria infection rates (Brugueras et al., 2020; Kulkarni et al., 2022; Lafferty, 2009; Mordecai et al., 2020). Climate change influences various environmental factors, including temperature, humidity, and precipitation, and causes a wide range of extreme weather events and disasters. It also affects malaria transmission (Paaijmans et al., 2010) because malaria is a vector-borne infectious disease and environmental conditions impact the vector mosquitos. Evidence suggests that the relationship between temperature and the transmission of malaria by mosquitos is nonlinear (Johnson et al., 2015; Mordecai et al., 2013). Malaria transmission increases with temperature, peaks at a specific temperature, and then decreases (Mordecai et al., 2013). Therefore, climate change might aggravate malaria transmission in the near term and alleviate it in the long term if the global temperature continues to increase. Greenhouse gas (GHG) emissions are the main factor associated with climate change and the economy. The Intergovernmental Panel on Climate Change (IPCC) relies on Coupled Model Intercomparison Projects (CMIP) to predict future temperatures in three periods based on several future emission scenarios (IPCC, 2022). In the IPCC sixth assessment report (AR6), updated emission scenarios are derived from different socioeconomic assumptions, called shared socioeconomic pathways (SSPs) (IPCC, 2022; Riahi et al., 2017). Among several SSPs, four scenarios are well-researched, including SSP1-2.6, SSP2-4.5, SSP3-7.0, and SSP5-8.5. From SSP1-2.6 to SSP5-8.5, the GHG emission reductions gradually decrease, and the temperature further increases (IPCC, 2022). The SSP1-2.6 scenario predicts that the temperature increase will stabilize at approximately 1.8 °C by the end of the century, whereas in the SSP5-8.5 scenario, temperatures are predicted to grow by 4.4 °C or more by 2100. According to these different scenarios, in different periods, including the near term (2021–2040), the medium term (2041–2060), and the long term (2081–2100), the effects of temperature on malaria will be diverse. This article presents the global differences in malaria infection rates among these different temperature scenarios in three periods.

To estimate the relationship between temperature and PfPR₂₋₁₀, we built a spatial dataset with a 0.25-degree resolution, including PfPR₂₋₁₀, a series of temperature-related variables, normalized difference vegetation index (NDVI), population density, and per-capita gross domestic product (GDP). The temperature-related variables included the annual average temperature, annual average temperature squared, and standard deviation of the monthly average temperature in a specific year. We used the annual average temperature and annual average temperature squared because the relationship between malaria transmission and temperature is nonlinear and because malaria incidences have been found to peak at approximately 25 °C in laboratory environments (Johnson et al., 2015; Mordecai et al., 2013, 2020). Both extremely low and high temperatures are unsuitable for the survival of transmission vectors (Mordecai et al., 2013; Parham and Michael, 2010). In this way, the standard deviation of the monthly average temperature in a specific year also affects PfPR₂₋₁₀. Additionally, the relationships among variables might not be stationary at a global scale, so we use geographically weighted panel regression (GWPR) to capture the spatial heterogeneities of these relationships.

We estimate the differences in the global PfPR₂₋₁₀ among different climate change scenarios projected by the IPCC during several periods, assuming that all conditions remain constant except temperature. Because the relationship between temperature and PfPR₂₋₁₀ is nonlinear (Johnson et al., 2015; Mordecai et al., 2013), the same increase in temperature under various situations would disproportionately affect PfPR₂₋₁₀. Furthermore, since GWPR is a spatially nonstationary model, the coefficients of the relationship between temperature and PfPR₂₋₁₀ spatially vary. Hence, our analysis could more accurately grasp the impacts of climate change. The impacts of climate change on PfPR₂₋₁₀ are estimated by calculating the difference in the PfPR₂₋₁₀ predictions under four well-known GHG emission scenarios, including SSP1-2.6, SSP2-4.5, SSP3-7.0, and SSP5-8.5, as described by the IPCC AR6 (IPCC, 2022). However, PfPR₂₋₁₀ cannot be predicted directly in our

GWPR model, as precisely predicting other variables such as NDVI, population, and per-capita GDP in several future periods is difficult. Inaccuracies in the predictions of other variables would adversely affect the PfPR₂₋₁₀ estimations under different scenarios. We thus assume that all conditions are the same except temperature to avert the influence of other variables' predictions on the PfPR₂₋₁₀ results. Although this assumption is irrational because the different analyzed SSPs lead to diverse population distributions and economic statuses, it is an effective way to probe and extract the impacts of climate change on PfPR₂₋₁₀. We mainly focus on the differences in the predicted PfPR₂₋₁₀ between SSP1-2.6 and the other higher-temperature scenarios.

To further demonstrate the impacts of increased temperatures on malaria infections, we converted the potential PfPR₂₋₁₀ difference caused by the scenario shifts into malaria infection case changes (MICCs). The IPCC predicts population densities based on diverse scenarios in several periods. We use these predicted population densities to estimate the global change pattern of malaria infection cases attributed to GHG emission scenario shifts in the near term, the medium term, and the long term.

There is a critical need to grasp how future temperature changes will shape the global epidemiological pattern of malaria. This study aims to quantify the impacts of climate change on the malaria infection rate in all epidemic regions, estimate potential MICCs resulting from increased temperatures, and identify the areas that are most vulnerable to increased malaria rates due to climate change.

2. Materials

2.1. *Plasmodium falciparum* parasite rate (PfPR)

The ongoing Malaria Atlas Project (Bhatt et al., 2015; Weiss et al., 2019) offers malaria infection prevalence information annually in terms of the PfPR among 2- to 10-year-old children globally from 2000 to 2019 (Malaria Atlas Project website: <https://malariaatlas.org/explorer/#/>). This dataset contains a series of spatial grid data at a 5-km resolution, covering the regions from 60° N to 60° S. Malaria is widely transmitted in Africa, although the infection prevalence has apparently decreased throughout this century according to the ongoing malaria infection mapping project and WHO report (Bhatt et al., 2015; Weiss et al., 2019; WHO, 2021). To make the spatial resolution of the PfPR data concordant with that of the climatic dataset, we upscale the spatial resolution of this dataset to 0.25 arc degrees by the averaging method. Fig. S1 shows the spatial distribution of the temporally averaged PfPR₂₋₁₀ values from 2000 to 2019. Although the coverage of the contemporary malaria control inventions skyrocketed during this period (Bhatt et al., 2015), the public health conditions regarding malaria infection in developing countries, especially in Sub-Saharan African countries, were still remarkably weak (WHO, 2021). For example, even in 2019, PfPR₂₋₁₀ was still over 60% in many Sub-Saharan African regions according to the Malaria Atlas Project.

2.2. Temperature

Temperature data are extracted from a United States National Aeronautics and Space Administration (NASA) dataset called NASA Global Land Data Assimilation System Version 2 (GLDAS-2.1). The GLDAS-2.1 system is based on a combination of modelled and observed data collected from 2000 to the present; these products represent a variety of monthly average climatic variables at a 0.25-arc-degree spatial resolution (Rodell et al., 2004). First, we obtain several climatic variables from GLDAS-2.1, including temperature, air pressure, absolute humidity, precipitation and wind speed. These variables are all provided as monthly average values and have subsequently been converted into annual average values. However, the correlations among these climatic variables are excessively high, and inputting all variables would thus lead to multicollinearity in the regressions. For example, the correlation

coefficient between the annual average air pressure and temperature is 0.745 (*p value* < 0.1%). Additionally, another critical independent variable, the vegetation index, is significantly correlated with absolute humidity (correlation coefficient: 0.807, *p value* < 0.1%), precipitation (0.805, *p value* < 0.1%) and wind speed (-0.716, *p value* < 0.1%). Therefore, only the annual average temperature is kept among the five climatic variables. Second, evidence shows that malaria transmission through *Anopheles gambiae* peaks at 25 °C (Mordecai et al., 2020). Hence, the relationship between the malaria infection rate and temperature is nonlinear and similar to an inverted U-shape (Johnson et al., 2015; Mordecai et al., 2013, 2019). We thus take the temperature-squared data into account. Furthermore, extremely low and high temperatures are unsuitable for the survival of malaria transmission vectors. In this way, the standard deviation of the monthly average temperature in a specific year would also affect the PfPR. In terms of climate, three variables, including the annual average temperature, annual average temperature squared, and standard deviation of the monthly average temperature in a specific year, are incorporated into the analysis.

2.3. Vegetation index

Local vegetation affects the malaria vector population size, survival, and biting rate, among other factors (Brugueras et al., 2020; Lourenço et al., 2011; Reiner et al., 2015). Therefore, the local vegetation status should be considered in this analysis. The NDVI is a widely used indicator applied to assess the extent to which an observed grid contains live green vegetation (Amadi et al., 2018; Midekisa et al., 2012). NDVI values range from -100% (no live green vegetation) to 100% (full of live green vegetation). The Moderate-resolution Imaging Spectroradiometer (MODIS) instruments onboard the Terra and Aqua satellites provide monthly NDVI data from 2000 to the present at a 0.05-arc-degree spatial resolution. The MODIS vegetation index products used in the analysis are MOD13C2 and MYD13C2 (Didan et al., 2015). To link the NDVI dataset to the temperature and PfPR₂₋₁₀ datasets, we upscale the NDVI dataset to a spatial resolution of 0.25 arc degrees by the averaging method. Then, these data are further converted into annual average values.

2.4. Population density and per-capita GDP

Population density data are obtained from the WorldPop Project. The WorldPop Project provides a spatially gridded dataset of population counts from 2000 to 2020 at a 1-km resolution (Linard et al., 2012; Sorichetta et al., 2015). Because the lengths of latitude lines decrease with increasing latitude, the conversion of the population counts from the 1-km resolution to the 0.25-arc-degree resolution is not perfect, or at least, the direct sum method cannot be used for this conversion. To solve this issue, we regard the population count in each grid cell as the population density and consider the unit of this dataset as the capita per square kilometer (Cap/km²). Then, we upscale the data resolution from 1 km to 0.25 arc degree by the averaging method. The dataset eventually illustrates the annual population density at a 0.25-arc-degree resolution.

The per-capita GDP is associated with the development level and public health investment of a region. A relatively high development level and more public health investments, including a wide range of international aids, are linked with a relatively low malaria infection rates (Bhatt et al., 2015; WHO, 2021). However, no spatially gridded per-capita GDP dataset is publicly available. We thus employ the country-level per-capita GDP provided by the World Bank. The unit of these per-capita GDP data is the current U.S. dollar. We assume that the per-capita GDP in each grid cell is consistent throughout each country.

2.5. Climate change scenarios and temperature prediction

The malaria infection rate is associated with temperature (Johnson

et al., 2015; Mordecai et al., 2013, 2020). The different climate change scenarios definitely lead to diverse malaria infection rates, assuming that the other conditions remain constant. The IPCC relies on the CMIP to predict future temperatures based on several future emission scenarios (IPCC, 2014; IPCC, 2022). The 2013 IPCC fifth assessment report (AR5) features four representative concentration pathways (RCPs) established according to various possible future GHG emissions (IPCC, 2014). Based on the RCPs and the CMIP Phase 5 (CMIP5) model, the IPCC projects four well-known scenarios, specifically RCP2.6, RCP4.5, RCP6.0, and RCP8.5. These scenarios are the updated version of the four scenarios established in the IPCC AR5, so the new scenarios listed in the IPCC AR6 are named SSP1-2.6, SSP2-4.5, SSP3-7.0, and SSP5-8.5 and are projected by the CMIP Phase 6 (CMIP6) model (IPCC, 2022). Except for SSP3-7.0, the other three scenarios are advanced from the previous scenarios in AR5. The SSP1-2.6 scenario predicts that the temperature increase will stabilize at approximately 1.8 °C by the end of the century. In the SSP2-4.5 scenario, the temperature is predicted to rise by 2.7 °C by 2100. According to the SSP3-7.0 scenario, the temperature will increase by approximately 3.6 °C by the end of the century. Finally, the SSP5-8.5 scenario predicts that the temperature will grow by 4.4 °C or higher by 2100. The IPCC projects global temperatures in three periods, including 2021–2040 (near term), 2041–2060 (medium term), and 2081–2100 (long term), based on the different scenarios described above. In each period, the dataset contains 12 gridded datapoints corresponding to monthly average temperatures. The IPCC provides open-access data based on simulations conducted with ensembles containing over 30 models at a 1-arc-degree resolution (<https://interactive-atlas.ipcc.ch/>). Furthermore, the IPCC also offers predicted population density gridded data produced through models simulations at a 1-arc-degree resolution. We obtain population density data projected under SSP2-4.5, SSP3-7.0, and SSP5-8.5 in the three future periods listed above.

2.6. Grids

We integrate the abovementioned dataset to build a long-panel spatially gridded dataset. Because we focus only on endemic areas, the grids in which PfPR₂₋₁₀ is always 0 are dropped. Additionally, every grid is required to have at least two years of complete records. Grids without sufficiently long records are also removed. Accordingly, 65,705 grids are kept. The coverage of our study exceeds 40 million km² based on the assumption that each grid cell covers 770 km². According to statistical tests and data availability, our analysis includes temperature, NDVI, population density, and per-capita GDP. Previous studies indicate that climate change affects vector-borne diseases (Altizer et al., 2013; Buchwald et al., 2020; Rogers and Randolph, 2006), so temperature-related variables and NDVI are considered herein. Moreover, population density and malaria-control interventions also play a critical role in malaria transmission (Bhatt et al., 2015; Nyaruaba et al., 2019). As detailed prevention investment data are unavailable, we replace them with the per-capita GDP.

3. Methods

3.1. Spatially stationary model

We assume that the relationships between PfPR₂₋₁₀ and the other selected independent variables are consistent among the grid cells in spatially stationary models. For example, the marginal effects of a 1% NDVI increase in Africa and South America are the same, even though these areas are thousands of kilometers apart. Without considering any spatial contexts, these relationships do not vary spatially (Brunsdon et al., 1998; Fotheringham et al., 2002). To estimate the links among variables, we apply the panel regression method. Because our dataset is a panel dataset, the hypotheses regarding time-fixed effects in each grid cell should be carefully tested. Three typical panel regression models

based on different time-fixed effect hypotheses, including the fixed-effects model (FEM), random-effects model (REM), and pooled ordinary-least-square (POLS) model, are widely used. We perform several statistical tests to select the most reasonable spatially stationary model. First, we execute the F test to explore individual effects (Breusch and Pagan, 1980; Croissant and Millo, 2008). The significant result indicates that time-fixed effects exist, as the null hypothesis is that no time-fixed effects are needed (Breusch and Pagan, 1980). Hence, the POLS model is rejected because this model assumes that no time-fixed effects exist. Then, we implement the Hausman test to determine whether the REM or FEM is reasonable (Kang, 1985). The null hypothesis of the Hausman test stating that the preferred model is the REM is rejected due to the significant test results. Therefore, the FEM is preferred in the spatially stationary analysis performed herein.

Here, the FEM is illustrated as follows:

$$PfPR_{it} = \beta X'_{it} + \alpha_i + \mu_{it} \quad (1)$$

where $PfPR_{it}$ denotes the annual $PfPR_{2-10}$ (ranging from 0 to 1) in grid i in year t , X_{it} denotes a matrix of independent variables, including the annual average temperature ($^{\circ}\text{C}$), annual average temperature squared ($^{\circ}\text{C}^2$), standard deviation of the monthly average temperature in year t ($^{\circ}\text{C}$), NDVI, population density (Cap/km^2), and per-capita GDP (USD/Cap) in measurement i in year t , α_i denotes the time-fixed effects, μ_{it} denotes an idiosyncratic error, and β is a vector of parameters to be estimated.

3.2. Spatially nonstationary model

Obviously, the marginal effects of the climatic variables on the malaria infection rate are not always, and potentially never, spatially consistent in the real world. For instance, Giesen et al. summarized the impacts of climate change on malaria in Africa in their review (Giesen et al., 2020). The marginal effects of climate change differ among countries (Alonso et al., 2011; Giesen et al., 2020; Murdock et al., 2016). There are two possible reasons to explain the difference. First, the relationship between climate change and the malaria infection rate is nonlinear (Johnson et al., 2015; Mordecai et al., 2013, 2019, 2020). To solve this issue, we employ the squared-temperature term. Second, the association of the malaria infection rate with temperature varies spatially (Kulkarni et al., 2022). The advanced spatially nonstationary model is thus employed to grasp this spatial variability.

GWPR was developed as an improved geographically weighted regression (GWR) method; GWPR allows regression coefficients to vary spatially (Brunsdon et al., 2010; Fotheringham and Oshan, 2016; Li and Managi, 2022) and is widely used in spatial analyses. Basically, in the GWPR method, the total dataset is divided into a large number of subdatasets according to the optimal bandwidth. The bandwidth of the GWPR is a threshold distance used to judge whether two grids have a spatial relationship (Beenstock and Felsenstein, 2019; Brunsdon et al., 1998, 2010). The number of subdatasets is equal to the number of grids. Each subdataset adopts one grid as its center and the bandwidth as the radius to select other grids. Of note, each grid could be utilized several times in this dividing process. Bandwidth calibration is an essential step in the analysis. The mean square prediction error of the regression is the critical index used to calibrate the bandwidth. The lowest mean square prediction error corresponds to the highest goodness of fit (Gollini et al., 2015). In the GWPR bandwidth calibration, the mean square prediction error is calculated as follows:

$$MSPE(b) = \frac{m \sum_j [y_j - \widehat{y}_j(b)]^2}{(m - p + 1)^2} \quad (2)$$

where $MSPE(b)$ is the mean square prediction error when the bandwidth is b , m is the data size, y_j is the dependent variable of the j th record, $\widehat{y}_j(b)$ is the predicted value of the j th record when the bandwidth is b , and p is

the number of the parameters in the analysis. Previous studies in which GWR, the basic version of GWPR, was used generally assumed that Equation (2) characterizes a U-shape function without statistical or mathematical evidence (Brunsden et al., 1998; Fotheringham et al., 2002; Gollini et al., 2015). This assumption helps reduce the calculation time but also introduces enormous risks to the analysis.

We apply the step increment selection method without assuming that Equation (2) characterizes a U-shape function. The bandwidth selection extent spans from 0.25 to 20 arc degrees, and the examined bandwidth increases by 0.25 arc degrees each iteration because the spatial resolution of the grid data is 0.25 arc degrees. The optimal bandwidth is found to be 4.25 arc degrees (Fig. S2). The mean square prediction error reaches the minimum value when the bandwidth is equal to 0.75, but we reject this result. According to the spatial resolution of the gridded dataset, each subdataset has at most 25 grids, but some subdatasets may have only one grid. If a subdataset has only one grid, it does not meet the statistical requirements of the FEM. Moreover, some grids might not be spatially linked with other grids at the 0.75-arc-degree bandwidth, lowering the robustness of the GWPR results. Therefore, the optimal bandwidth, 4.25 arc degrees, is used in the calibration process.

GWPR is performed after the optimal bandwidth has been calibrated. The GWPR model is written as follows:

$$PfPR_{it} = \beta_i X'_{it} + \alpha_i + \varepsilon_{it} \quad (3)$$

where β_i denotes a vector of parameters in the regression with the subdataset taking the grid i as the center. There are 65,705 subdatasets, so the number of subdataset regressions is also 65,705, and each estimation is based on the spatial weight vector of the corresponding subdataset. For this reason, the parameters, β_i , vary spatially. The spatial weight vector is calculated as follows:

$$W_i = \begin{cases} \left[1 - \left(\frac{d}{b} \right)^2 \right]^2, & d_k \in d \text{ if } d_k \leq b \\ 0, & d_k \notin d \text{ if } d_k > b \end{cases} \quad (4)$$

where W_i denotes a vector of spatial weights between grid i and its neighbors, d represents a vector of distances between grid i and its neighbors, b is the calibrated optimal bandwidth, and d_k is the distance between grid i and grid k . Then, in the GWPR process, the parameters are estimated based on the derived spatial weight vectors. Because the time-fixed effects term (α_i) is unknown in Equation (3) (Croissant and Millo, 2008), we transform that equation as follows:

$$PfPR_{it} - \overline{PfPR}_i = \beta_i (X_{it} - \overline{X}_i)' + (\varepsilon_{it} - \overline{\varepsilon}_i) \quad (5)$$

where \overline{PfPR}_i denotes the mean $PfPR_{2-10}$ value in grid i , \overline{X}_i denotes a vector of the mean independent variables of grid i , and $\overline{\varepsilon}_i$ denotes the mean error in grid i . To simplify Equation (5), we define the matrix of transformed independent variables x_{it} and the transformed dependent variable pfp_{it} as follows:

$$x_{it} = X_{it} - \overline{X}_i \quad (6)$$

$$pfp_{it} = PfPR_{it} - \overline{PfPR}_i \quad (7)$$

$$\sigma_{it} = \varepsilon_{it} - \overline{\varepsilon}_i \quad (8)$$

In light of Equations (6)–(8), Equation (3) is rewritten as follows:

$$pfp_{it} = \beta_i x'_{it} + \sigma_{it} \quad (9)$$

The parameter estimation method can thus be displayed as follows:

$$\beta_i = [x_{it}^T W_i x_{it}]^{-1} x_{it}^T W_i pfp_{it} \quad (10)$$

3.3. Statistical indicators and 10-fold cross-validation

Because we need to make predictions based on the IPCC stimulation results, we must first confirm the accuracy of the selected model. Several statistical indicators, including R^2 , the root mean square error (RMSE), the mean absolute error (MAE), the correlation coefficient (r) between observed and predicted values, and the regression coefficients between the observed and predicted values (intercept α and slope β), are applied to depict the accuracy of the model. R^2 is a critical statistical indicator describing the goodness of fit and is expressed as follows:

$$R^2 = 1 - \frac{\sum_{k=1}^n (OPfPR_k - PPfPR_k)^2}{\sum_{k=1}^n (OPfPR_k - \bar{OPfPR})^2} \quad (11)$$

where n represents the number of observations in the whole dataset, $OPfPR_k$ represents the k th record of the observed PfPR₂₋₁₀ value, $PPfPR_k$ represents the k th record of the predicted PfPR₂₋₁₀ value, and \bar{OPfPR} represents the mean observed PfPR₂₋₁₀ value. The RMSE is sensitive to both systematic error and random errors and can be expressed as follows:

$$RMSE = \sqrt{\frac{1}{n} \sum_{k=1}^n (OPfPR_k - PPfPR_k)^2} \quad (12)$$

3.4. The MAE is computed as follows

$$MAE = \text{mean}(|OPfPR_k - PPfPR_k|) \quad (13)$$

In the analysis, the MAE is expected to be relatively lower. Additionally, the regression coefficients between the observed and predicted values are estimated as follows:

$$OPfPR_k = \alpha + \beta PPfPR_k + \delta_k \quad (14)$$

where α is the intercept of the regression, the ideal value of which is 0; β is the slope, the ideal value of which is 1; and δ_k is a random error term.

To assess the reliability of the GWPR model, we perform a 10-fold cross-validation. In this 10-fold cross-validation, the whole dataset is randomly divided into ten subdatasets. In each individual cross-validation iteration, nine subdatasets are used to train the GWPR model, while the remaining subdataset is employed to test the accuracy and prediction ability of the model. All statistical indicators, including R^2 , RMSE, MAE, r , α , and β , are reported based on the training and testing results.

3.5. Effects of temperature change on PfPR₂₋₁₀

The effects of temperature changes on PfPR₂₋₁₀ cannot be directly estimated because other necessary variables, such as NDVI, the population, and the per-capita GDP, cannot be precisely predicted. The errors arising from predicting these other variables would drastically affect the PfPR₂₋₁₀ estimations. However, if we assume that these other variables remain constant among the various scenarios, we can extract the differences in the impacts of temperature changes among different periods. The difference between two temperature scenarios is calculated as follows:

$$\Delta PfPR_{it} = S2PfPR_{it} - S1PfPR_{it} \quad (15)$$

where $\Delta PfPR_{it}$ denotes the difference between the PfPR₂₋₁₀ estimations obtained under two different temperature scenarios in grid i during period t , $S1PfPR_{it}$ denotes the PfPR₂₋₁₀ estimations obtained based on temperature scenario $S1$ in grid i during period t , and $S2PfPR_{it}$ denotes the PfPR₂₋₁₀ estimation obtained based on temperature scenario $S2$ in grid i during period t . We hope to obtain the impacts of relatively high GHG emissions on PfPR₂₋₁₀, so the SSP1-2.6 scenario is always set as temperature scenario $S1$, while one of the other three scenarios,

including SSP2-4.5, SSP3-7.0, and SSP5-8.5, is set as temperature scenario $S2$.

To estimate $S1PfPR_{it}$ and $S2PfPR_{it}$, we expand Equation (3) as follows:

$$\begin{aligned} S1PfPR_{it} &= \beta_{1i} TeS1'_{it} + \beta_{2i} TeS1^2'_{it} + \beta_{3i} TSDS1'_{it} + \beta_{4i} NDVI'_{it} + \beta_{5i} POP'_{it} \\ &\quad + \beta_{6i} GDP'_{it} + \alpha_i \end{aligned} \quad (16)$$

$$\begin{aligned} S2PfPR_{it} &= \beta_{1i} TeS2'_{it} + \beta_{2i} TeS2^2'_{it} + \beta_{3i} TSDS2'_{it} + \beta_{4i} NDVI'_{it} + \beta_{5i} POP'_{it} \\ &\quad + \beta_{6i} GDP'_{it} + \alpha_i \end{aligned} \quad (17)$$

where $\beta_{1i}, \beta_{2i}, \beta_{3i}, \beta_{4i}, \beta_{5i}$, and β_{6i} are components of the estimated GWPR parameter vector β_i from Equation (10), $TeS1_{it}$ denotes the annual average temperature simulated under the SSP1-2.6 scenario in grid i during period t , $TSDS1_{it}$ denotes the standard deviation of the monthly average temperature simulated under the SSP1-2.6 scenario in grid i during period t , $TeS2_{it}$ denotes the annual average temperature simulated under the other scenario in grid i during period t , $TSDS2_{it}$ denotes the standard deviation of the monthly average temperature under the other scenario in grid i during the period t , and $NDVI_{it}$, POP_{it} , and GDP_{it} denote the NDVI, population density, and per-capita GDP in grid i during period t , respectively.

In view of Equations (16) and (17), Equation (15) is rewritten and simplified as follows:

$$\begin{aligned} \Delta PfPR_{it} &= \beta_{1i}(TeS2_{it} - TeS1_{it})' + \beta_{2i}(TeS2^2_{it} - TeS1^2_{it})' \\ &\quad + \beta_{3i}(TSDS2_{it} - TSDS1_{it})' \end{aligned} \quad (18)$$

3.6. Differences in infection cases among different scenarios

In this work, we estimate the infection case changes resulting from shifts in development scenarios based on the predicted PfPR₂₋₁₀ differences between different scenarios. In this study, the predicted dependent variable is PfPR₂₋₁₀, but the IPCC does not provide population data of 2- to 10-year-old children. Hence, we assume that the PfPR comprising all ages is the same as PfPR₂₋₁₀ to predict infection case changes. Although this assumption might bias the results, the residuals are limited and acceptable. In Africa, parasite prevalence in 0.5- to 4-year-old children is 10.1%, similar to the overall rate of 9.9% obtained on the coast of Kenya (Kamau et al., 2020). Furthermore, in Asia, the age factor does not significantly affect malaria prevalence (Nguiragool et al., 2019; Ramdzan et al., 2020). The PfPR is calculated as the clinical incidence rate rather than the rate of symptomatic infection or the case fatality rate, both of which are strongly affected by sex and age (Rajahram et al., 2019). The case fatality rate is significantly associated with age because adults' immune systems are stronger than children's, but the prevalence rate is not associated with age. Therefore, PfPR₂₋₁₀ could represent the all-age PfPR to some degree. The infection case changes can be estimated as follows:

$$\Delta ICC_{itk} = \Delta PfPR_{itk} \times Population_{itk} \quad (19)$$

where ΔICC_{itk} denotes the infection case change due to a k shift in development scenarios in grid i during period t , $\Delta PfPR_{itk}$ denotes the difference resulting from a k shift in development scenarios in grid i during period t estimated by Equation (18), and $Population_{itk}$ denotes the IPCC-predicted population in grid i during period t under the relatively high-temperature scenario in the k shift. Three development scenario shifts are considered: the shift from SSP1-2.6 to SSP2-4.5, from SSP1-2.6 to SSP3-7.0, and from SSP1-2.6 to SSP5-8.5.

4. Results

4.1. Impacts of climate change in the near term (2021–2040)

From 2021 to 2040, the global average PfPR₂₋₁₀ difference between SSP2-4.6 and SSP1-2.6 is 0.164% (with a 95% uncertainty interval [UI] of 0.160%–0.168%). This difference is associated with a 6.506 (6.150–6.861) million increase in malaria infection cases. Compared to the WHO-reported infection case number of 241 million cases in 2020, this finding represents a 2.699% increase. Among the continents, the average differences range from –0.076% (–0.063% to –0.090%) in Europe to 0.409% (0.400%–0.418%) in Africa during the 2021–2040 period (Table 1). The global average difference between SSP3-7.0 and SSP1-2.6 is 0.104% (0.101%–0.107%), which corresponds to a 3.655 (3.416–3.894) million increase in malaria infection cases, or a 1.517% increase based on the number of infection cases reported in 2020. The average PfPR₂₋₁₀ difference between SSP3-7.0 and SSP1-2.6 is significantly increased in Oceania and South America compared to the differences between SSP2-4.6 and SSP1-2.6, while in Africa, Asia, and Europe, the values tend to decrease. North America has few grids in the analysis, so the impacts of increased temperatures are marginal in these regions. The global average difference between SSP5-8.5 and SSP1-2.6 is 0.041% (0.038%–0.044%) in the near term, correlated with a 2.823 (2.635–3.012) million increase in cases or a 1.171% increase according to the reported infection case numbers in 2020. It must be underscored that even though the difference between SSP5-8.5 and SSP1-2.6 in Africa is numerically smaller than the differences found in the other two comparisons, the value is still positive. Thus, from 2021 to 2040, in

Africa, the PfPR₂₋₁₀ will increase by 0.139% (0.132%–0.146%) under SSP5-8.5 compared to under SSP1-2.6, while these values will rise by 0.409% (0.400%–0.418%) and 0.258% (0.251%–0.265%) under SSP2-4.5 and SSP3-7.0, respectively. In summary, in the near term, increased temperatures negatively impact malaria infection globally, and the most vulnerable region, Africa, might be most affected by climate change. The places most affected by increased temperatures often do not coincide with areas of high population densities. For each continent, the average MICCs resulting from a shift in development scenarios differ from the average PfPR₂₋₁₀ differences (Table 2). From 2021 to 2040, increased temperatures will affect the African epidemic region the most. On average, the malaria infection cases are expected to increase by 0.329 (0.312–0.347), 0.189 (0.178–0.201), and 0.147 (0.137–0.156) case/km² due to the shifts from SSP1-2.6 to SSP2-4.5, to SSP3-7.0, and to SSP5-8.5, respectively.

Fig. 1 demonstrates the national average difference between the two different scenarios in each set from 2021 to 2040. According to this figure, most African countries will be adversely affected by the higher-temperature scenarios, including SSP2-4.5, SSP3-7.0, and SSP5-8.5. For example, the difference between SSP2-4.5 and SSP1-2.6 is highest in Togo in the near term, at 2.041% (1.873%–2.208%). The situations in Burkina Faso and Ghana are slightly better, at 2.020% (1.927%–2.113%) and 1.693% (1.437%–1.772%), respectively. Evidence shows that these three countries were affected the most by malaria from 2000 to 2015 (Bhatt et al., 2015). In contrast, in the near term, the relatively high-temperature scenarios might reduce the PfPR₂₋₁₀ values in some other places due to the nonlinear relationship assumption and local regression technology. Gabon and Equatorial Guinea are cases in point.

Table 1
Average PfPR₂₋₁₀ differences between SSP 1–2.6 and other scenarios.

	Continent	From SSP1-2.6 to SSP 2–4.5	UI	From SSP1-2.6 to SSP 3–7.0	UI	From SSP1-2.6 to SSP 5–8.5	UI
2021–2040	Africa	0.409%	(0.400%– 0.418%)	0.258%	(0.251%– 0.265%)	0.139%	(0.132%–0.146%)
	Asia	0.003%	(0.002%– 0.003%)	0.000%	(0.000%– 0.001%)	–0.005%	(–0.006%–0.005%)
	Europe	–0.076%	(–0.090%– 0.063%)	–0.115%	(–0.127%– 0.103%)	–0.300%	(–0.324%–0.276%)
	North America	0.000%	(0.000%– 0.000%)	0.000%	(0.000%– 0.000%)	0.000%	(0.000%–0.000%)
	Oceania	0.002%	(–0.002%– 0.007%)	0.009%	(0.001%– 0.018%)	–0.023%	(–0.030%–0.017%)
	South America	0.003%	(0.003%– 0.004%)	0.006%	(0.005%– 0.007%)	–0.038%	(–0.039%–0.037%)
2041–2060	Africa	–0.376%	(–0.386%– 0.366%)	–1.065%	(–1.089%– 1.040%)	–1.601%	(–1.637%–1.564%)
	Asia	–0.013%	(–0.013%– 0.012%)	–0.026%	(–0.027%– 0.024%)	–0.043%	(–0.046%–0.041%)
	Europe	–0.605%	(–0.647%– 0.563%)	–1.300%	(–1.390%– 1.211%)	–1.850%	(–1.983%–1.716%)
	North America	0.000%	(0.000%– 0.000%)	0.000%	(–0.001%– 0.000%)	–0.001%	(–0.001%–0.000%)
	Oceania	–0.040%	(–0.053%– 0.027%)	–0.070%	(–0.093%– 0.046%)	–0.134%	(–0.183%–0.084%)
	South America	–0.086%	(–0.088%– 0.083%)	–0.158%	(–0.163%– 0.153%)	–0.299%	(–0.308%–0.290%)
2081 - 2100	Africa	–2.888%	(–2.952%– 2.824%)	–6.696%	(–6.858%– 6.534%)	–8.769%	(–8.989%–8.549%)
	Asia	–0.070%	(–0.074%– 0.066%)	–0.147%	(–0.156%– 0.138%)	–0.205%	(–0.219%–0.191%)
	Europe	–2.809%	(–3.020%– 2.599%)	–7.284%	(–7.807%– 6.761%)	–10.894%	(–11.686%– 10.101%)
	North America	–0.001%	(–0.002%– 0.001%)	–0.003%	(–0.004%– 0.001%)	–0.005%	(–0.008%–0.003%)
	Oceania	–0.188%	(–0.257%– 0.119%)	–0.378%	(–0.537%– 0.220%)	–0.548%	(–0.784%–0.311%)
	South America	–0.366%	(–0.377%– 0.355%)	–1.020%	(–1.052%– 0.989%)	–1.697%	(–1.748%–1.645%)

Note: The SSP1-2.6 scenario is used as the baseline to demonstrate the impacts of climate change. The estimation of the PfPR₂₋₁₀ differences is conducted following Eqs. (15)–(18).

Table 2
MICCs resulting from shifts in development scenarios.

	Continent	From SSP1-2.6 to SSP 2-4.5	UI	From SSP1-2.6 to SSP 3-7.0	UI	From SSP1-2.6 to SSP 5-8.5	UI
2021–2040	Africa	0.329	(0.312–0.347)	0.189	(0.178–0.201)	0.147	(0.137–0.156)
	Asia	-0.009	(-0.010 to -0.007)	-0.011	(-0.012 to -0.009)	-0.008	(-0.009 to -0.007)
	Europe	-0.001	(-0.002 - 0.000)	-0.003	(-0.005 to -0.002)	-0.011	(-0.015 to -0.006)
	North America	0.000	(0.000–0.000)	0.000	(0.000–0.000)	0.000	(0.000–0.000)
	Oceania	-0.001	(-0.002 - 0.000)	-0.002	(-0.004 - 0.000)	-0.002	(-0.003 - 0.000)
	South America	0.000	(0.000–0.000)	-0.001	(-0.001 - 0.000)	-0.001	(-0.001 to -0.001)
2041–2060	Africa	-0.362	(-0.383 to -0.342)	-1.210	(-1.277 to -1.142)	-1.279	(-1.358 to -1.201)
	Asia	-0.016	(-0.018 to -0.015)	-0.036	(-0.039 to -0.033)	-0.025	(-0.031 to -0.018)
	Europe	-0.031	(-0.044 to -0.017)	-0.074	(-0.106 to -0.042)	-0.088	(-0.128 to -0.048)
	North America	0.000	(-0.001 - 0.000)	-0.001	(-0.001 - 0.000)	-0.001	(-0.002 to -0.001)
	Oceania	-0.003	(-0.006 - 0.000)	-0.009	(-0.015 to -0.003)	-0.007	(-0.018 - 0.004)
	South America	-0.002	(-0.003 to -0.002)	-0.006	(-0.009 to -0.004)	-0.008	(-0.010 to -0.005)
2081–2100	Africa	-3.883	(-4.105 to -3.661)	-11.690	(-12.357 to -11.024)	-7.978	(-8.567 to -7.389)
	Asia	-0.070	(-0.085 to -0.054)	-0.211	(-0.248 to -0.174)	-0.135	(-0.175 to -0.095)
	Europe	-0.167	(-0.242 to -0.091)	-0.618	(-0.887 to -0.349)	-0.468	(-0.685 to -0.252)
	North America	-0.002	(-0.003 to -0.001)	-0.008	(-0.011 to -0.005)	-0.006	(-0.008 to -0.004)
	Oceania	-0.014	(-0.032 - 0.005)	-0.030	(-0.088 - 0.027)	-0.018	(-0.065 - 0.029)
	South America	-0.010	(-0.013 to -0.006)	-0.038	(-0.051 to -0.025)	-0.035	(-0.048 to -0.023)

Note: the unit of this table is case/km².

In Gabon, the PfPR₂₋₁₀ difference between SSP2-4.5 and SSP1-2.6 is -0.531% (-0.578% to -0.483%), and in Equatorial Guinea, this difference is -0.276% (-0.389% to -0.483%). Regarding the PfPR₂₋₁₀ differences between SSP3-7.0 and SSP1-2.6, the highest value is found in Burkina Faso, at 1.391% (1.359%–1.423%). The change from SSP3-7.0 to SSP1-2.6 reduces the malaria infection rate to the greatest extent in Gabon, at -0.411% (-0.450% to -0.372%) and in Equatorial Guinea, at -0.406% (-0.502% to -0.310%). Additionally, in Togo, the PfPR₂₋₁₀ difference between SSP5-8.5 and SSP1-2.6 is the largest across the globe, at 1.604% (1.439%–1.772%). The situations in Burkina Faso and Ghana are slightly better than that in Togo, with values of 1.592% (1.503%–1.682%) and 1.301% (1.211%–1.390%), respectively. On the other hand, in Mozambique and Zimbabwe, the effect of the change from SSP1-2.6 to SSP5-8.5 on PfPR₂₋₁₀ decreases the malaria infection rate. In Mozambique, the difference between SSP5-8.5 and SSP1-2.6 is -0.530% (-0.553% to -0.507%), and in Zimbabwe, this value is -0.379% (-0.403% to -0.354%).

4.2. Impacts of climate change in the medium term (2041–2060)

From 2041 to 2060, the global average PfPR₂₋₁₀ differences between SSP2-4.5 and SSP1-2.6, between SSP3-7.0 and SSP1-2.6, and between SSP5-8.5 and SSP1-2.6 are -0.181% (-0.185% to -0.177%), -0.482% (-0.493% to -0.472%), and -0.730% (-0.762% to -0.730%), respectively. These differences are associated with MICCs of -7.541 (-7.968 to -7.115) million, -24.892 (-26.264 to -23.520) million, and -26.164 (-27.761 to -24.568) million, corresponding to changes of -3.129%, -10.329%, and -10.857%, respectively, compared to the infection case number reported in 2020. On all continents, the change from a low-temperature to a higher-temperature scenario reduces the PfPR₂₋₁₀ (Tables 1 and 2). The differences in PfPR₂₋₁₀ between SSP2-4.5 and SSP1-2.6 in Africa, Asia, Oceania, and South America in the medium

term become negative, though the same values obtained in the near term are positive. This indicates that the effects of temperatures on the PfPR₂₋₁₀ have exceeded the turning point in most areas (Mordecai et al., 2013). The increased temperatures lead to potential decreases in malaria infection due to the creation of unsuitable environments for the survival of malaria vectors (Parham and Michael, 2010). Even though, in most regions, relatively high-temperature scenarios are associated with lower PfPR₂₋₁₀ values, the temperature increases do adversely affect PfPR₂₋₁₀ in some countries (Fig. 2). For example, the difference in PfPR₂₋₁₀ between SSP2-4.5 and SSP1-2.6 in Gabon is 0.926% (0.837%–1.014%). In terms of reducing malaria infections, Mozambique still benefits most from the scenario change from SSP1-2.6 to SSP2-4.5, with a case reduction of -1.924% (-1.970%–1.878%). It must be noted that this temperature increase significantly slashes the malaria infection rates in the countries that have historically been most critically affected by malaria, such as Burkina Faso and Togo, in the medium term.

4.3. Impacts of climate change in the long term (2081–2100)

In the long term, the global average PfPR₂₋₁₀ differences between SSP2-4.5 and SSP1-2.6, between SSP3-7.0 and SSP1-2.6, and between SSP5-8.5 and SSP1-2.6 are -1.287% (-1.315% to -1.260%), -3.036% (-3.105% to -2.967%), and -4.096% (-4.190% to -4.002%), respectively; these differences correspond to MICCs of -79.109 (-83.626 to -74.591) million, -238.337 (-251.920 to -224.754) million, and -162.693 (-174.628 to -150.757) million, denoting percent changes of -32.825%, -98.895%, and -67.507%, respectively, according to the infection case number reported in 2020. Because the increased temperatures exceed turning point in the effects of temperature increase on PfPR₂₋₁₀ in most areas, the positive impacts of temperature increases with regards to controlling malaria infections are expected to rise in these scenarios (Tables 1 and 2). In this case, the

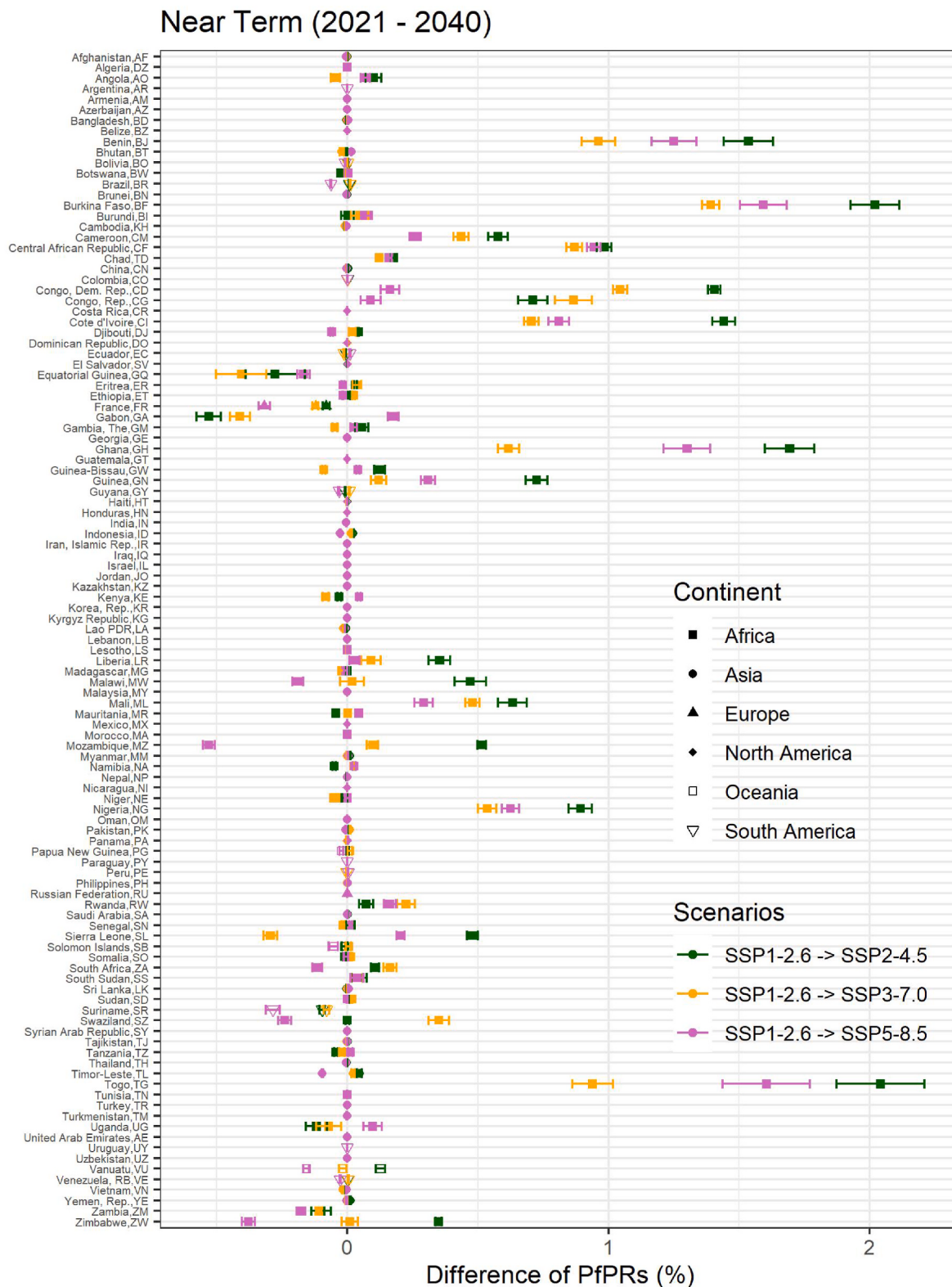


Fig. 1. PfPR₂₋₁₀ differences from 2021 to 2040.

positive impacts of the increased temperatures on PfPR₂₋₁₀ peak under SSP5-8.5 during the 2081–2100 period. However, it must be emphasized that even though, on average, the whole world benefits from these high temperatures, some countries will experience increased suffering. For instance, in Gabon, the PfPR₂₋₁₀ difference between SSP2-4.5 and SSP1-2.6 reaches 4.991% (4.346%–5.636%), the difference between SSP3-7.0

and SSP1-2.6 reaches 9.317% (7.554%–11.080%), and the difference between SSP5-8.5 and SSP1-2.6 reaches to 10.701% (8.092%–13.309%), as shown in Fig. 3.

Fig. 4 illustrates the grid-level MICCs obtained under the three scenario shifts during the three considered periods. Briefly, the spatial distribution shows that epidemics in the Sub-Saharan African countries

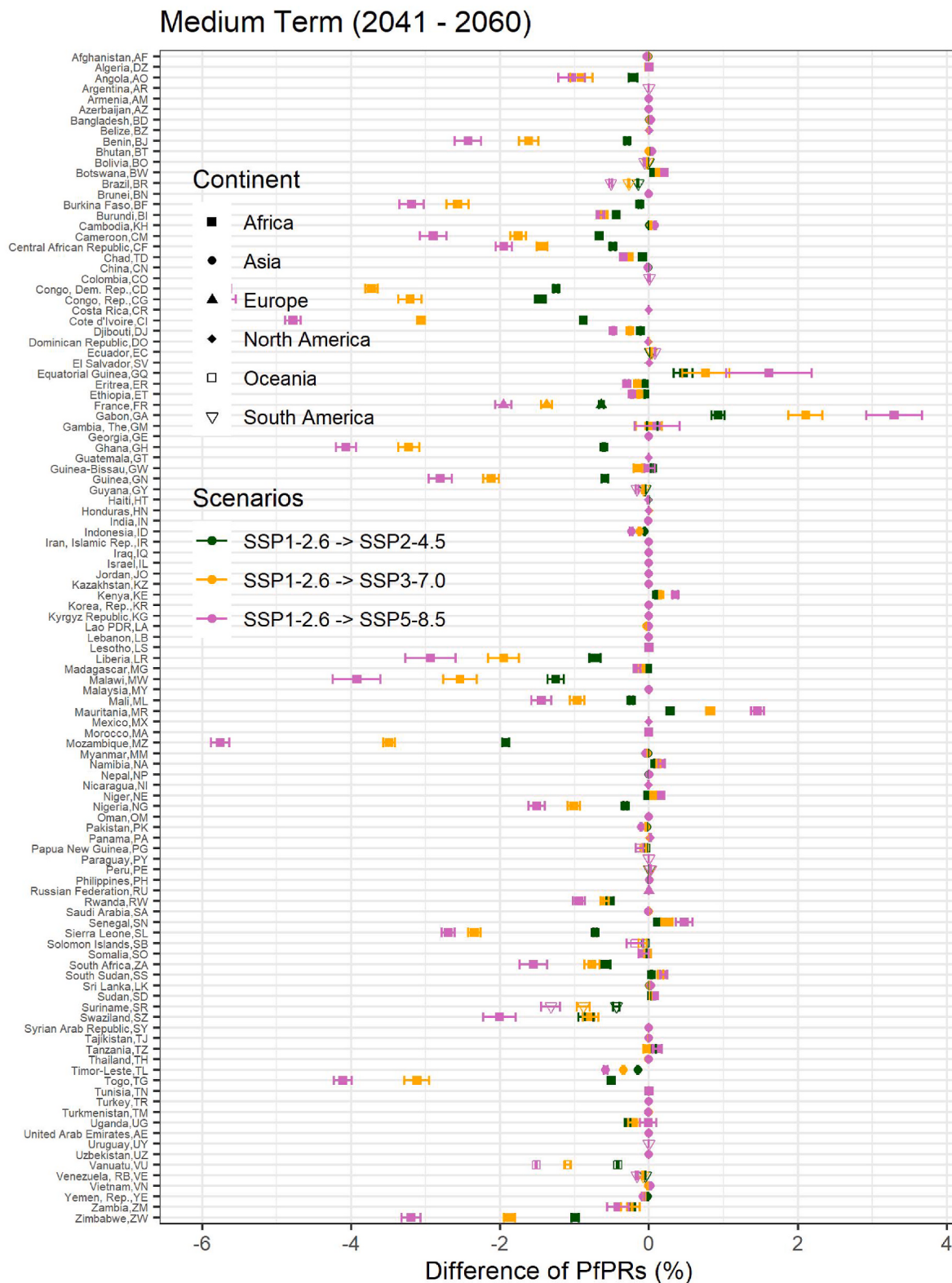


Fig. 2. PfPR₂₋₁₀ differences from 2041 to 2060.

are most sensitive to climate change. There are two reasons for this sensitivity. First, the coefficients of the relationship between temperature and PfPR₂₋₁₀ are numerically larger in Africa than in other continents. Second, with climate change, the temperatures increase the most in Africa. In the medium- and long-terms scenarios, the PfPR₂₋₁₀ reductions in Africa seemingly benefit from the higher-temperature

scenarios, but this benefit should be treated carefully due to the assumption that all other variables will remain constant.

5. Discussion

In the 0.25-arc-degree grid-level analysis, the utilized GWPR model

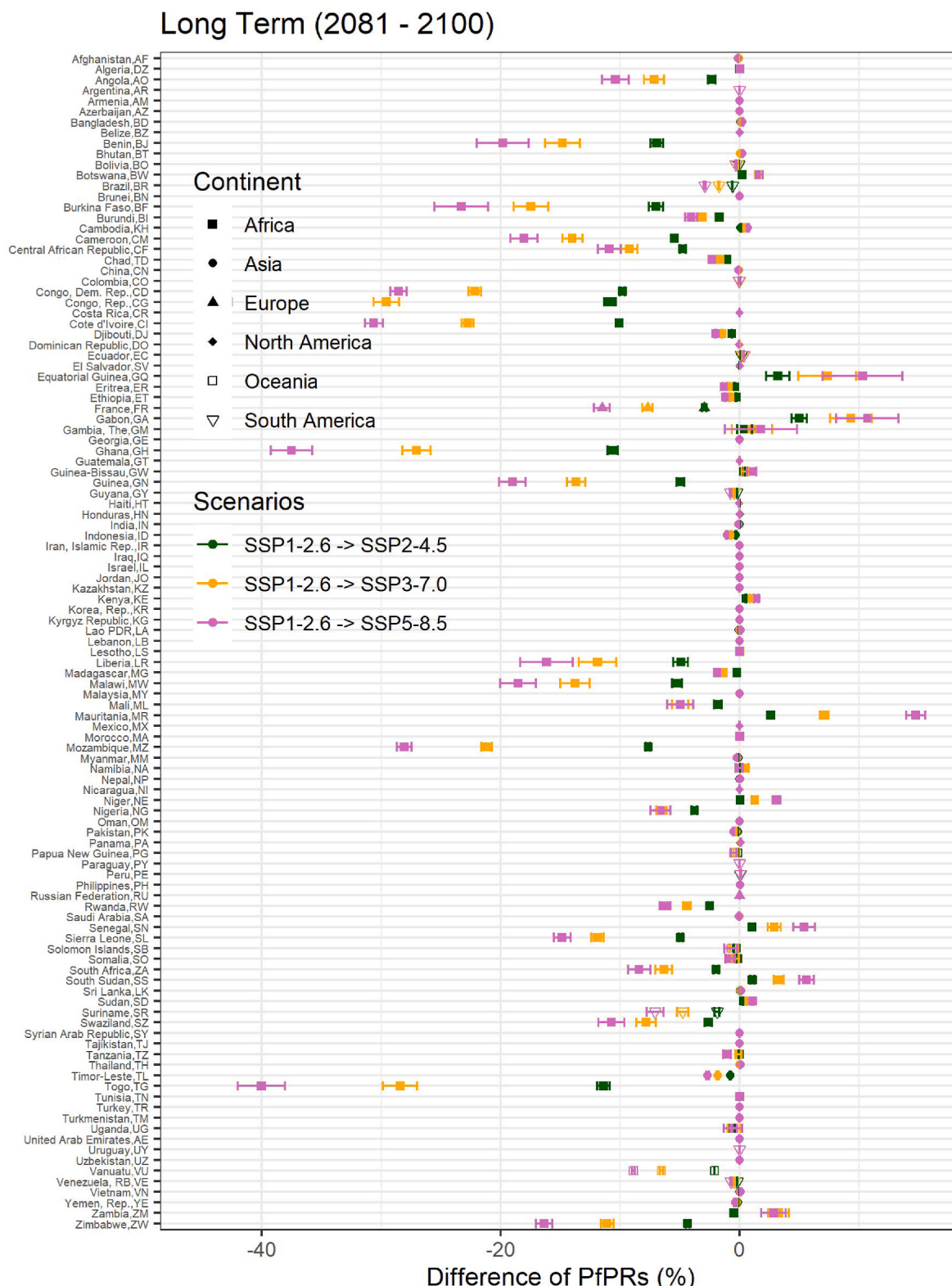


Fig. 3. PfPR₂₋₁₀ differences from 2081 to 2100.

leads to robust and accurate estimates of the impacts of climate change on PfPR₂₋₁₀. The accuracy of the GWPR model is 94.75%. In the 10-fold cross-validation, the goodness of fit of every single iteration is over 94%, indicating high robustness. Detailed information about the cross-validation process is reported in the **appendix**. The main contributors to the accurate estimates obtained in our analysis are the PfPR₂₋₁₀ data

disclosed by the Malaria Atlas Project (Bhatt et al., 2015), the climatic data provided by NASA (Rodell et al., 2004), and the understanding of the nonlinear relationship between the malaria infection rate and temperature obtained with the availability of recent evidence (Johnson et al., 2015; Mordecai et al., 2013, 2020). Based on this highly accurate model, the influence of temperature scenario changes on malaria

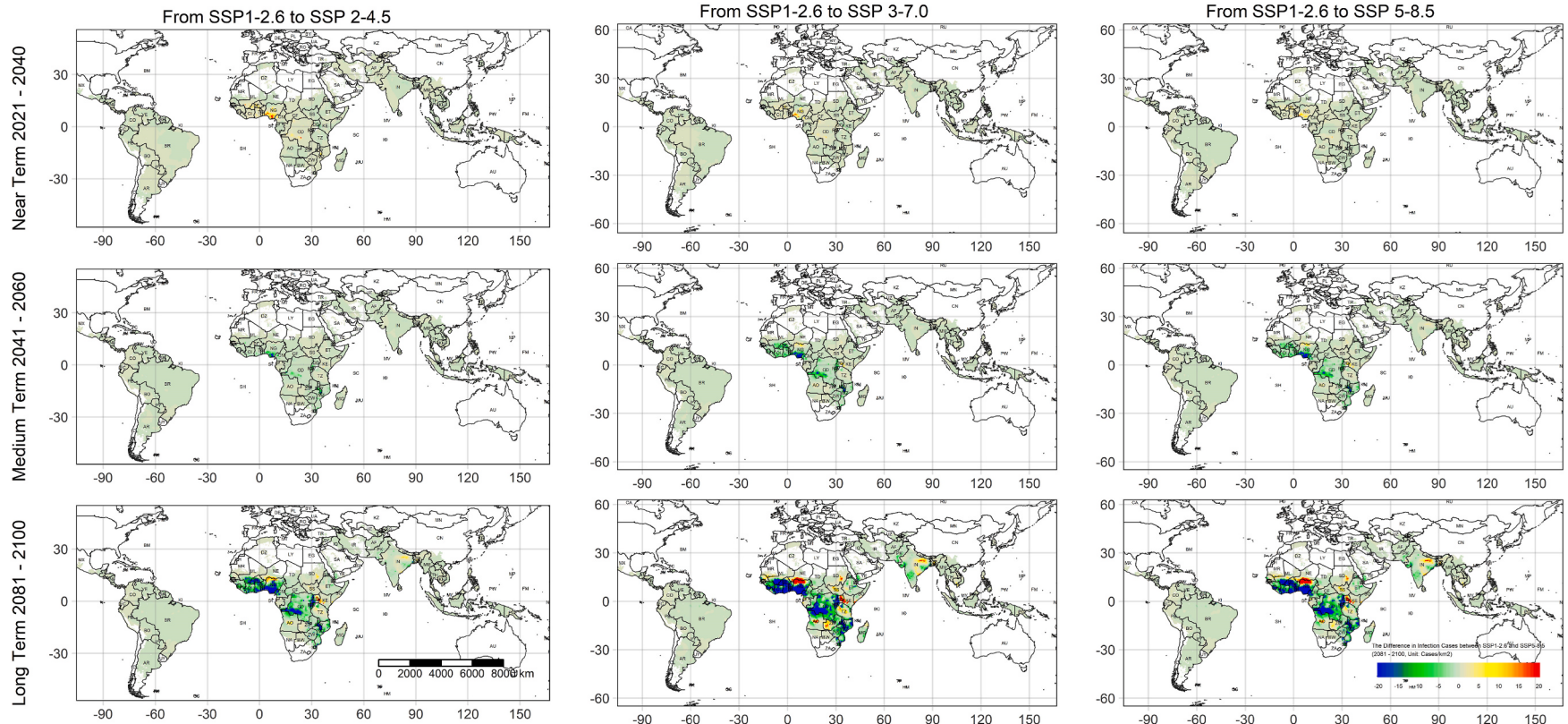


Fig. 4. Grid-level MICCs identified in three scenario shifts and in three different periods.

prevalence can be isolated and extracted. In the near term, substantial temperature increases lead to increased PfPR₂₋₁₀ values, especially in the most vulnerable region, namely, Africa. However, in the medium and long terms, further temperature increases are predicted to drastically ameliorate the PfPR₂₋₁₀.

Extremely high temperatures are definitely not an effective or efficient way to control malaria, especially high temperatures resulting as a byproduct of climate change. Biologically, extremely high temperatures are not suitable environmental conditions for the survival or propagation of arbovirus vectors (Mordecai et al., 2019). Therefore, on the surface, extremely high temperatures can be thought to curb the malaria infection rate. However, the effects of high temperatures on human health are also severely adverse. First, various diseases, such as cardiovascular diseases (Hu et al., 2021), mental health diseases (Lee et al., 2018) and other nontransmissible diseases, are linked with high temperatures. Evidence shows that 0.54% of global deaths were attributable to high temperatures in 2019 (Song et al., 2021). In the SSP5-8.5 scenario, by 2100, the annual average temperature in Africa is expected to exceed 27 °C, and the average temperature in summer is predicted to be approximately 30 °C. Obviously, in this case, most areas in Africa would not be livable. Second, agriculture will also be hit by extreme weather under severe climate change scenarios (Anyamba et al., 2014). In Africa, hunger is still a critical issue (Mason-D'Croz et al., 2019). An increase in temperatures would directly result in plummeting local food production. More people would suffer from hunger, and the growth of more children would be stunted (Mason-D'Croz et al., 2019). Third, natural environments would also be adversely affected under this scenario. Anthropogenic climate change caused desertification in more than 5 million km² from 1982 to 2015, and African countries were affected the most (Burrell et al., 2020). Furthermore, biodiversity and sustainability would be slashes, which could induce other transmissible epidemics in addition to vector-borne diseases, such as the novel coronavirus COVID-19 (Lawler et al., 2021). In the medium and long terms, increased temperatures might result in dwindled PfPR₂₋₁₀ values globally, but we must treat this situation carefully because the negative impacts resulting from high temperatures in other aspects are unacceptable.

In the near term, the relatively high-temperature scenarios, including SSP2-4.5, SSP3-7.0, and SSP5-8.5, would potentially elicit PfPR₂₋₁₀ increases mainly in Africa. The WHO aims to reduce the malaria case incidence by at least 90% by 2030 relative to the 2000 level and to eliminate malaria in at least 35 countries by 2030 (WHO, 2021). However, high temperatures will be a negative factor in this period, as increased temperatures make the environment more suitable for malaria vectors. Although even in the most sustainable scenario, namely, SSP1-2.6, the temperature will rise to the peak temperature for malaria transmission, efforts to achieve SSP1-2.6 will delay the arrival of this peak temperature. In other words, efforts to combat climate change can buy more time for organizations, mainly the WHO, to eliminate malaria. With no or limited malaria infections and enough prevention against the re-establishment of malaria (WHO, 2021), the re-establishment of malaria will be impossible, even though the temperature conditions will be ideal for epidemic outbreaks. In this way, decreasing GHG emissions and curbing malaria incidence rates in the near term are the most reasonable and practical approaches to reducing the prevalence of malaria, rather than relying on the extremely high temperatures that will accompany climate change in the future.

In the medium term, increased temperatures reduce the PfPRs in African regions near the equator because the temperatures in those areas are predicted to exceed the most suitable value for malaria transmission. Malaria has hit these areas worst in the past 20 years. Favorable environmental factors, including temperature and humidity conditions, are crucial for mosquitos (Lyons et al., 2014; Santos-Vega et al., 2022). With increased temperatures, these suitable environments will move to relatively high-latitude and coastal areas. Obviously, relatively high-latitude and coastal areas, which are expected to have relatively low-temperature and high-humidity conditions in the medium and long

terms, are more suitable for malaria vectors than other regions. With these changes in the spatial distribution of malaria vectors, the malaria prevalence pattern would, in turn, change.

Our study has several limitations. The PfPR₂₋₁₀ differences between two scenarios are obtained based on the strong assumption that all conditions except for temperature-related variables will remain constant in all scenarios. However, societal and economic conditions would be diverse under different scenarios, according to the SSP definition and the IPCC AR6 (IPCC, 2022). Although GHG emission reductions mainly influence the populations and economies of developed countries, the malaria epidemics in developing countries will also be impacted to some degree. Moreover, greenness is associated with temperature (Burrell et al., 2020; Lamchin et al., 2018). High temperatures cause desertification in the most vulnerable ecosystems, especially those in Africa (Burrell et al., 2020).

Our analysis assumes that the relationship between temperature and PfPR₂₋₁₀ is nonlinear, according to previous evidence (Johnson et al., 2015; Mordecai et al., 2013; Parham and Michael, 2010). This nonlinear association is commonly characterized by a U-shape, although this assumption is imperfect, as, in the real world, this relationship is more complex than our assumption. Capturing a more complex relationship may further improve the accuracy of our predictions, even though the accuracy of our model is 94.75%. In future studies, machine learning methods, such as artificial neural networks and ridge regression, could be combined with GWR to further probe this relationship. Furthermore, the temporal resolution considered herein is the annual resolution, which results in underestimated short-term effects of temperature changes, e.g., monthly or even real-time effects. Although we employ the annual standard deviation of monthly temperatures, the improvement is marginal.

This study is also limited by gaps in the available malaria-control intervention data. We consider only one indicator, the per-capita GDP, to represent the prevention ability because no long-term, reasonable-spatial-resolution malaria-control intervention information is available for most non-African countries. Moreover, the utilized per-capita GDP data are recorded at the country level. Even though we take this into account, the heterogeneities within countries are ignored in our analysis. For this reason, unfortunately, we cannot estimate the economic losses resulting from the impacts of increased temperature on malaria, which could be substantial.

In conclusion, climate change would increase the danger and risk of malaria in the most vulnerable regions in the near term. This study provides an impetus for policymakers to limit warming to a reasonable value. To achieve the ideal end to the malaria elimination process, engaging civil societies and the public to reduce GHG emissions represents a potential way to help those threatened by malaria. Because the peak optimal temperature for malaria transmission will be reached regardless in some regions, malaria elimination should be completed and prioritized in those areas.

Declaration of competing interest

The authors declare that they have no known competing financial interests or personal relationships that could have appeared to influence the work reported in this paper.

Data availability

All data sources used in the analyses, along with fully reproducible code, are publicly available at https://github.com/MichaelChaoLi-cpu/Malaria_And_Climate_Change.

Acknowledgement

This research was supported by the following funding agencies: Japan Society for the Promotion of Science (Grant No. JP20H00648),

the Environment Research and Technology Development Fund of the Environmental Restoration and Conservation Agency of Japan (Grant No. JPMEEFR20201001), and also Japan Science and Technology Agency (Grant No. JPMJSP2136). The statistical analyses were carried out using the computer resources offered under the category of General Projects by the Research Institute for Information Technology, Kyushu University, Japan.

Appendix A. Supplementary data

Supplementary data to this article can be found online at <https://doi.org/10.1016/j.envres.2022.114028>.

References

- Alonso, D., Bouma, M.J., Pascual, M., 2011. Epidemic malaria and warmer temperatures in recent decades in an East African highland. *Proc. Biol. Sci.* 278, 1661–1669.
- Altizer, S., Ostfeld Richard, S., Johnson Pieter, T.J., Kutz, S., Harvell, C.D., 2013. Climate change and infectious diseases: from evidence to a predictive framework. *Science* 341, 514–519.
- Amadi, J.A., Olago, D.O., Ong'Amo, G.O., Oriaso, S.O., Nanyangi, M., Nyamongo, I.K., et al., 2018. Sensitivity of vegetation to climate variability and its implications for malaria risk in Baringo, Kenya. *PLoS One* 13, e0199357.
- Anyamba, A., Small, J.L., Britch, S.C., Tucker, C.J., Pak, E.W., Reynolds, C.A., et al., 2014. Recent weather extremes and impacts on agricultural production and vector-borne disease outbreak patterns. *PLoS One* 9, e92538.
- Beenstock, M., Felsenstein, D., 2019. The Econometric Analysis of Non-stationary Spatial Panel Data. Springer.
- Bhatt, S., Weiss, D.J., Cameron, E., Bisanzio, D., Mappin, B., Dalrymple, U., et al., 2015. The effect of malaria control on Plasmodium falciparum in Africa between 2000 and 2015. *Nature* 526, 207–211.
- Breusch, T.S., Pagan, A.R., 1980. The Lagrange multiplier test and its applications to model specification in econometrics. *Rev. Econ. Stud.* 47, 239.
- Bruguera, S., Fernández-Martínez, B., Martínez-De La Puente, J., Figueroa, J., Porro, T. M., Rius, C., et al., 2020. Environmental drivers, climate change and emergent diseases transmitted by mosquitoes and their vectors in southern Europe: a systematic review. *Environ. Res.* 191, 110038.
- Brundson, C., Fotheringham, A.S., Charlton, M.E., 2010. Geographically weighted regression: a method for exploring spatial nonstationarity. *Geogr. Anal.* 28, 281–298.
- Brundson, C., Fotheringham, S., Charlton, M., 1998. Geographically weighted regression. *J. Roy. Stat. Soc.: Ser. D (The Statistician)* 47, 431–443.
- Buchwald, A.G., Hayden, M.H., Dadzie, S.K., Paull, S.H., Carlton, E.J., 2020. Aedes-borne disease outbreaks in West Africa: a call for enhanced surveillance. *Acta Trop.* 209, 105468.
- Burrell, A.L., Evans, J.P., De Kauwe, M.G., 2020. Anthropogenic climate change has driven over 5 million km² of drylands towards desertification. *Nat. Commun.* 11, Croissant, Y., Millo, G., 2008. Panel data econometrics in R: the plm package. *J. Stat. Software* 27.
- Didan, K., Munoz, A.B., Solano, R., Huete, A., 2015. University of Arizona: Vegetation Index Phenology Lab. MODIS Vegetation Index User's Guide. MOD13 series.
- Fotheringham, A., Brundson, C., Charlton, M., 2002. Geographically Weighted Regression: the Analysis of Spatially Varying Relationships, vol. 13. John Wiley & Sons.
- Fotheringham, A.S., Oshan, T.M., 2016. Geographically weighted regression and multicollinearity: dispelling the myth. *J. Geogr. Syst.* 18, 303–329.
- Giesen, C., Roche, J., Redondo-Bravo, L., Ruiz-Huerta, C., Gomez-Barroso, D., Benito, A., et al., 2020. The impact of climate change on mosquito-borne diseases in Africa. *Pathog. Glob. Health* 114, 287–301.
- Gollini, I., Lu, B., Charlton, M., Brundson, C., Harris, P., 2015. GWmodel: an R package for exploring spatial heterogeneity using geographically weighted models. *J. Stat. Software* 63.
- Hu, J., Hou, Z., Xu, Y., Zhou, M., Zhou, C., Xiao, Y., et al., 2021. Life loss of cardiovascular diseases per death attributable to ambient temperature: a national time series analysis based on 364 locations in China. *Sci. Total Environ.* 756, 142614.
- IPCC, 2014. Climate Change 2014 Synthesis Report. IPCC, Geneva, Switzerland.
- IPCC, 2022. Climate Change 2022: Impacts, Adaptation and Vulnerability.
- Johnson, L.R., Ben-Horin, T., Lafferty, K.D., McNally, A., Mordecai, E., Paaijmans, K.P., et al., 2015. Understanding uncertainty in temperature effects on vector-borne disease: a Bayesian approach. *Ecology* 96, 203–213.
- Kamau, A., Mtanje, G., Mataza, C., Mwambingu, G., Mturi, N., Mohammed, S., et al., 2020. Malaria infection, disease and mortality among children and adults on the coast of Kenya. *Malar. J.* 19.
- Kang, S., 1985. A note on the equivalence of specification tests in the two-factor multivariate variance components model. *J. Econom.* 28, 193–203.
- Kulkarni, M.A., Duguay, C., Ost, K., 2022. Charting the evidence for climate change impacts on the global spread of malaria and dengue and adaptive responses: a scoping review of reviews. *Glob. Health* 18.
- Lafferty, K.D., 2009. The ecology of climate change and infectious diseases. *Ecology* 90, 888–900.
- Lamchin, M., Lee, W.-K., Jeon, S.W., Wang, S.W., Lim, C.H., Song, C., et al., 2018. Long-term trend and correlation between vegetation greenness and climate variables in Asia based on satellite data. *Sci. Total Environ.* 618, 1089–1095.
- Lawler, O.K., Allan, H.L., Baxter, P.W.J., Castagnino, R., Tor, M.C., Dann, L.E., et al., 2021. The COVID-19 pandemic is intricately linked to biodiversity loss and ecosystem health. *Lancet Planet. Health* 5, e840–e850.
- Lee, S., Lee, H., Myung, W., Kim, E.J., Kim, H., 2018. Mental disease-related emergency admissions attributable to hot temperatures. *Sci. Total Environ.* 616–617, 688–694.
- Li, C., Managi, S., 2022. Estimating monthly global ground-level NO₂ concentrations using geographically weighted panel regression. *Rem. Sens. Environ.* 280, 113152.
- Linard, C., Gilbert, M., Snow, R.W., Noor, A.M., Tatem, A.J., 2012. Population distribution, settlement patterns and accessibility across Africa in 2010. *PLoS One* 7, e31743.
- Lourenço, P.M., Sousa, C.A., Seixas, J., Lopes, P., Novo, M.T., Almeida, A.P.G., 2011. Anopheles atroparvus density modeling using MODIS NDVI in a former malarious area in Portugal. *J. Vector Ecol.* 36, 279–291.
- Lyons, C.I., Coetzee, M., Terblanche, J.S., Chown, S.L., 2014. Desiccation tolerance as a function of age, sex, humidity and temperature in adults of the African malaria vectors *Anopheles arabiensis* Patton and *Anopheles funestus* Giles. *J. Exp. Biol.* 217, 3823–3833.
- Mason-D'Croz, D., Sulser, T.B., Wiebe, K., Rosegrant, M.W., Lowder, S.K., Nin-Pratt, A., et al., 2019. Agricultural investments and hunger in Africa modeling potential contributions to SDG2 – zero Hunger. *World Dev.* 116, 38–53.
- Midekisa, A., Senay, G., Henebry, G.M., Semuniguse, P., Wimberly, M.C., 2012. Remote sensing-based time series models for malaria early warning in the highlands of Ethiopia. *Malar. J.* 11, 165.
- Mordecai, E.A., Caldwell, J.M., Grossman, M.K., Lippi, C.A., Johnson, L.R., Neira, M., et al., 2019. Thermal biology of mosquito-borne disease. *Ecol. Lett.* 22, 1690–1708.
- Mordecai, E.A., Paaijmans, K.P., Johnson, L.R., Balzer, C., Ben-Horin, T., De Moor, E., et al., 2013. Optimal temperature for malaria transmission is dramatically lower than previously predicted. *Ecol. Lett.* 16, 22–30.
- Mordecai, E.A., Ryan, S.J., Caldwell, J.M., Shah, M.M., Labeaud, A.D., 2020. Climate change could shift disease burden from malaria to arboviruses in Africa. *Lancet Planet. Health* 4, e416–e423.
- Murdock, C.C., Sternberg, E.D., Thomas, M.B., 2016. Malaria transmission potential could be reduced with current and future climate change. *Sci. Rep.* 6, 27771.
- Nguiragool, W., Karl, S., White, M., Koepfli, C., Felger, I., Singhasivanon, P., et al., 2019. Highly heterogeneous residual malaria risk in western Thailand. *Int. J. Parasitol.* 49, 455–462.
- Nyaruaba, R., Mwaliko, C., Mwau, M., Mousa, S., Wei, H., 2019. Arboviruses in the East African Community partner states: a review of medically important mosquito-borne Arboviruses. *Pathog. Glob. Health* 113, 209–228.
- Paaijmans, K.P., Blanford, S., Bell, A.S., Blanford, J.I., Read, A.F., Thomas, M.B., 2010. Influence of climate on malaria transmission depends on daily temperature variation. *Proc. Natl. Acad. Sci.* 107, 15135–15139.
- Parham, P.E., Michael, E., 2010. Modeling the effects of weather and climate change on malaria transmission. *Environ. Health Perspect.* 118, 620–626.
- Rajahram, G.S., Cooper, D.J., William, T., Grigg, M.J., Anstey, N.M., Barber, B.E., 2019. Deaths from *Plasmodium knowlesi* malaria: case series and systematic review. *Clin. Infect. Dis.* 69, 1703–1711.
- Ramdzan, A.R., Ismail, A., Mohd Zanib, Z.S., 2020. Prevalence of malaria and its risk factors in Sabah, Malaysia. *Int. J. Infect. Dis.* 91, 68–72.
- Reiner, R.C., Geary, M., Atkinson, P.M., Smith, D.L., Gething, P.W., 2015. Seasonality of *Plasmodium falciparum* transmission: a systematic review. *Malar. J.* 14.
- Riahi, K., Van Vuuren, D.P., Kriegler, E., Edmonds, J., O'Neill, B.C., Fujimori, S., et al., 2017. The Shared Socioeconomic Pathways and their energy, land use, and greenhouse gas emissions implications: an overview. *Global Environ. Change* 42, 153–168.
- Rodell, M., Houser, P.R., Jambor, U., Gottschalck, J., Mitchell, K., Meng, C.J., et al., 2004. The global land data assimilation system. *Bull. Am. Meteorol. Soc.* 85, 381–394.
- Rogers, D.J., Randolph, S.E., 2006. Climate change and vector-borne diseases. In: Hay, S. I., Graham, A., Rogers, D.J. (Eds.), Advances in Parasitology. 62. Academic Press, pp. 345–381.
- Santos-Vega, M., Martinez, P.P., Vaishnav, K.G., Kohli, V., Desai, V., Bouma, M.J., et al., 2022. The neglected role of relative humidity in the interannual variability of urban malaria in Indian cities. *Nat. Commun.* 13.
- Song, J., Pan, R., Yi, W., Wei, Q., Qin, W., Song, S., et al., 2021. Ambient high temperature exposure and global disease burden during 1990–2019: an analysis of the Global Burden of Disease Study 2019. *Sci. Total Environ.* 787, 147540.
- Sorichetta, A., Hornby, G.M., Stevens, F.R., Gaughan, A.E., Linard, C., Tatem, A.J., 2015. High-resolution gridded population datasets for Latin America and the Caribbean in 2010, 2015, and 2020. *Sci. Data* 2, 150045.
- Weiss, D.J., Lucas, T.C.D., Nguyen, M., Nandi, A.K., Bisanzio, D., Battle, K.E., et al., 2019. Mapping the global prevalence, incidence, and mortality of *Plasmodium falciparum*, 2000–17: a spatial and temporal modelling study. *Lancet* 394, 322–331.
- WHO, 2021. World Malaria Report 2021.